



## The Finite-interval Spectral Power method for detecting underground cavities using seismic ambient noise

Journal:	<i>Geophysical Journal International</i>
Manuscript ID:	GJI-20-0413.R1
Manuscript Type:	Research Paper
Date Submitted by the Author:	23-Jul-2020
Complete List of Authors:	Kristekova, Miriam; Slovak Academy of Sciences, Earth Science Institute; Comenius University in Bratislava Kristek, Jozef; Comenius University in Bratislava; Slovak Academy of Sciences, Earth Science Institute Moczo, Peter; Comenius University in Bratislava; Slovak Academy of Sciences, Earth Science Institute Labak, Peter; CTBTO
Keywords:	Seismic noise < SEISMOLOGY, Fourier analysis < GEOPHYSICAL METHODS, Statistical methods < GEOPHYSICAL METHODS, Earthquake monitoring and test-ban treaty verification < SEISMOLOGY

SCHOLARONE™  
Manuscripts

1  
2  
3       The Finite-interval Spectral Power method  
4  
5           for detecting underground cavities  
6  
7           using seismic ambient noise  
8  
9  
10  
11  
12  
13  
14  
15  
16  
17  
18  
19  
20  
21  
22  
23  
24  
25  
26  
27  
28  
29  
30  
31  
32  
33  
34  
35  
36  
37  
38  
39  
40  
41  
42  
43  
44  
45  
46  
47  
48  
49  
50  
51  
52  
53  
54  
55  
56  
57  
58  
59  
60

# The Finite-interval Spectral Power method for detecting underground cavities using seismic ambient noise

Miriam Kristekova<sup>1,2</sup>, Jozef Kristek<sup>2,1</sup>, Peter Moczo<sup>2,1</sup>, Peter Labak<sup>3</sup>

<sup>1</sup> *Earth Science Institute of the Slovak Academy of Sciences, Dubravská cesta 9, 840 05 Bratislava, Slovakia*

<sup>2</sup> *Comenius University in Bratislava, Mlynska dolina F1, 842 48 Bratislava, Slovakia*

<sup>3</sup> *CTBTO Preparatory Commission, Vienna International Centre, 1400 Vienna, Austria*

Submitted:

April 29, 2020

Revision submitted:

July 23, 2020

An abbreviated title:

The FISP method for detecting cavities

Corresponding author:

Jozef Kristek

Comenius University in Bratislava

Mlynska dolina F1

842 48 Bratislava

Slovakia

Phone: +421-2-60295337

Email: [kristek@fmph.uniba.sk](mailto:kristek@fmph.uniba.sk)

## SUMMARY

Undetected natural and man-made cavities pose a serious geotechnical hazard to human safety. It is therefore important to develop methods for identifying and locating underground cavities in urban development and civil construction. Another important type of cavity is the one generated by an underground nuclear explosion. Identification and location of such cavities is an important proof in case of suspicion of violating the Comprehensive Nuclear-Test-Ban Treaty (CTBT), an international treaty banning nuclear weapon test explosion or any other nuclear explosion which is yet to come into force. We present a new method for detecting and locating a horizontal position of cavity which uses the Finite-interval Spectral Power (FISP) of seismic ambient noise. The method makes it possible to use single-station measurements at a set of potentially irregularly distributed points in the area on the Earth's free surface over a suspected cavity. Because the method gives better results for undistorted segments of noise records, we also present a method of automatic identification of such segments. We tested our method using records of noise from a site near the Felsőpetény, Hungary, which were collected for the CTBT Organisation during a field test in the framework of developing on-site inspection (OSI) capabilities. The method is ready for further tests in different cavity conditions and applications.

**Key words:** Seismic noise; Fourier analysis; Statistical methods; Earthquake monitoring and test-ban treaty verification

## 1 INTRODUCTION

Underground cavities pose a serious geotechnical hazard to human safety, especially in highly urbanized town centres, urban development and civil construction. Depending on the historical development or natural underground conditions some areas are relatively rich of cavities. Cavities of natural origin are typical for karst regions. There are several types of man-made cavities. For example, as mentioned by Guidoboni et al. (2003), the ancient medieval towns in Italy are often built on old man-made underground cavities such as Roman underground water systems of aqueducts and cisterns, and medieval tunnels for storage and communications. Another type of cavities is due to mining activities. The natural and man-made cavities pose problem especially if they are not known or documented.

An interesting and important type of cavity is the one generated by an underground nuclear explosion. Identification and location of such cavities is an important finding in case of

suspicion of violating the CTBT. Because the Treaty bans nuclear explosions, reliable verification tools are required to make sure that no nuclear explosion goes undetected. In addition to the global monitoring system, a range of different inspection techniques and activities are permitted for use during OSIs including imaging, geophysical and radionuclide related techniques. Here we refer to important contributions by Sweeney & Harben (2010) and Sweeney & Mellors (2014) directly related to the CTBT activities.

Sweeney & Harben (2010) carried out a passive resonance seismometry experiment at the former Nevada Test Site. They deployed a line of sensors above an old underground nuclear test and a control line above undisturbed ground. They attempted various ways of analysing data but could see no clear difference between the signals recorded on both lines. For this experiment they used only vertical-component sensors and concluded that it would be better to use 3-component sensors because some of the techniques they tried may work better with the horizontal components of the wavefield.

Sweeney & Mellors (2014) used the electrical resistivity tomography/induced polarisation (ERT/IP) and controlled source audio magnetotellurics (CSAMT) methods to image an underground-nuclear-explosion cavity/rubble zone. They found that the ERT/IP technique was limited in the depth penetration and could not probe the region of the rubble chimney and/or explosion cavity. The CSAMT technique could resolve resistivity differences to a depth of 700m, but the emplacement hole casing had a large effect and masked deeper effects of the chimney or rubble zone. Sweeney & Mellors (2014) also used active seismic methods with a small vibroseis source for both compressional and shear waves. They were not able to use the vibroseis source directly above the cavity because of health and safety concerns of causing a collapse. Using refraction microtremor analysis techniques they were able to see a shear wave velocity anomaly in the vicinity of the expected rubble chimney zone. Traditional reflection processing techniques revealed possible reflections from the top and bottom of the rubble zone and some lateral discontinuities, but they were not easily distinguishable from the background reflections.

For successful application of seismological techniques, it is necessary to better understand effects of cavities on seismic wavefields. Sgarlato et al. (2011) studied the effects of the cave Grotta Petralia, Italy, and several artificial tunnels on local seismic response around the cavities. The cave has the total length about 500 m, its cross section has a variable size ranging between 10 and 15m in width, and is about 2.5 m high on average. The cave develops at a depth of about 3 m from the topographic surface and its easternmost part is open. It is formed by several chambers connected by tight passages and it shows evidence of several collapses. They analysed earthquake and seismic ambient noise records using spectral ratio techniques. They

observed spectral peaks in the frequency range 3.0–7.0 Hz in the local horizontal-to-vertical spectral ratios and in the standard site-to-reference spectral ratios. The spectral amplitudes decreased with increasing distance from the cavity and increasing depth of the cavity. The authors did not focus on identification and location of cavity based on the earthquake and seismic ambient noise records.

Sica et al. (2014) performed 2D numerical simulations for a model inspired by the village of Castelnuovo, Italy, which during the 2009 Abruzzo earthquake suffered large damage. The study indicated that the presence of multiple shallow cavities considerably affects ground motion amplification along the free surface of the hill.

Kolesnikov & Fedin (2018) and Filippi et al. (2019) presented nice overviews of geophysical techniques used for detecting and studying underground cavities. Ortiz-Aguilar & De Basabe (2020) presented a review of the numerical-modelling investigations of effects of cavities assuming different sources of seismic wavefield. As far as we know there is no numerical-modelling study investigating the effect of cavities on seismic ambient noise.

Kolesnikov & Fedin (2018) studied the possibilities of using seismic ambient noise for detection and delineation of near-surface cavities. Using laboratory modelling with acoustic noise excitation and field experiments they showed that the averaging of amplitude spectra of a large number of records makes it possible to find frequencies and amplitudes of compressional standing waves generated by noise in the space between the free surface and underground cavity. They concluded that presence of distinct regular spectral peaks is an evidence of the presence of an underground hollow or considerably low-velocity object. They investigated shallow (less than 3m) cavities in simple medium and they observed fading signature with increasing depth of cavity. No generalization to structurally more complex media was presented.

Our work was motivated by efforts to develop CTBT OSI capabilities to detect and locate cavities in underground medium altered by underground nuclear explosion in depths of possibly several hundreds of meters using resonance seismometry. Several authors (e.g., Kolesnikov & Fedin 2018, Korneev 2009, Korneev et al. 2014, Schneider et al. 2017) reported anomalies in spectral characteristics of seismic wavefields and related them to resonance effects due to the presence of a cavity. The observed spectral anomalies, however, can be masked or faded away in structurally more complex medium, more complex wavefield excitation and larger depth of cavity.

In case of a CTBT OSI, the inspection team would have limited time for the inspection techniques and activities at the site of a suspected underground nuclear explosion. The total number of available seismic instruments would also be limited, and the deployment of a

sufficiently large and dense array is unlikely. The limited time might be short for recording sufficient number of earthquakes. In addition to applicable active seismic methods it is obviously useful and important to have a robust method based on analysis of single-station records of ever-present seismic ambient noise.

Here we present a new method, which uses the Finite-interval Spectral Power (FISP) of seismic ambient noise for detecting and locating a horizontal position of underground cavities. Our method is a result of comprehensive and iterative investigation based on analysis of recorded seismic ambient noise in the structurally complex environment. The method does not assume array measurements. Because the method gives better results for undistorted segments of noise records, we also present a method of automatic identification of such segments using Tukey's fences applied to spectral power.

We tested the applicability of the method using records of seismic ambient noise obtained in the Felsőpetény area, Hungary, in 2019 in the framework of OSI field measurements.

## 2 PROPOSAL OF A NEW METHOD: A FINITE-INTERVAL SPECTRAL POWER (FISP)

In this section we explain the concept of the Finite-interval Spectral Power (FISP) of seismic ambient noise (for brevity we will further use only “noise” with the meaning of seismic ambient noise) and its use for detecting and locating underground cavities. We assume a set of potentially irregularly distributed measurement points in the area on the Earth’s free surface over a suspected cavity and sufficiently long 3-component records of noise at all measurement points. The records of noise should be obtained in similar measurement conditions but they can be performed sequentially.

As the first (preprocessing) step it is necessary to check quality of noise records and select only those segments of records with similar (stationary) characteristics, i.e., we need to identify and exclude the outliers. Having the stationary time segments selected, power spectral density (PSD) and the Finite-interval Spectral Power (FISP) for each measurement point can be calculated.

### 2.1. Tukey's fences applied to spectral power

Here we present a method of automatic identification of time segments of the entire noise record which are somehow distorted, e.g. by transient anthropogenic signals, and thus not usable for evaluating desired noise characteristics. The innovative principle of our approach is application of Tukey's fences to spectral power.

Note, that it is possible to exclude outlying time segments by a (manual) visual inspection of power spectrum for each segment individually. Obviously, however, in case of hundreds or even thousands of chosen segments, three components and tens of measurement points, the manual inspection of power spectrum of each segment is considerably laborious.

Assume that the entire noise record at each measurement point is divided into equal-duration time segments with 50% overlap. A segment should contain the largest period of interest at least 10 times. A wavelength corresponding to the largest period of interest should be close to the minimum linear dimension of the area covered by measurement points.

We multiply each segment by the Welch window. The Welch window is defined as

$$W(k) = 1 - \left( \frac{k - N/2}{N/2} \right)^2; \quad 0 \leq k \leq N \quad (1)$$

where  $N$  is the number of samples of the segment. We calculate a power spectrum for each tapered segment,  $|X_j(f)|^2$ ,  $j$  indicating the  $j^{\text{th}}$  segment. As in many other noise analyses, it is necessary to smooth the obtained power spectrum, e.g. using Konno-Ohmachi (1998) smoothing function

$$KO(f; f_c) = \left\{ \frac{\sin[b \log_{10}(f/f_c)]}{b \log_{10}(f/f_c)} \right\}^4 \quad (2)$$

The smoothed power spectrum as a function of frequency  $f_c$  is then calculated as

$$|\tilde{X}_j(f_c)|^2 = \sum_f [KO(f, f_c) |X_j(f)|^2]. \quad (3)$$

Then the spectral power of each segment is obtained as

$$SP_j = \int_{f_{\min}}^{f_{\max}} |\tilde{X}_j(f)|^2 df \quad (4)$$

where  $f_{\min} \approx 10/T_S$ ,  $T_S$  being duration of the segment, and  $f_{\max}$  depends on the maximum frequency of interest and/or parameters of data acquisition system used for measurements.

After eliminating outliers by laborious (manual) visual inspection of power spectra of all segments, we have found that the spectral power of remaining almost stationary noise has a log-normal distribution. The fact of the log-normal distribution makes it possible to replace the manual visual inspection by an automatic procedure. The procedure consists in application of

the Tukey's fences (also Tukey's rules, Tukey 1977) to  $\log(SP_j)$ . The principle of the Tukey's fences is illustrated in Fig. 1.

We propose the following method of automatic selection of almost stationary time segments of noise:

- 1 Division of the entire noise record into equal-duration time segments with 50% overlap.  
The segment should contain the largest period of interest at least 10 times.
- 2 Application of Welch window to each segment.
- 3 Computation of power spectrum of each segment.
- 4 Smoothing of power spectrum of each segment.**
- 5 Computation of spectral power of each segment.
- 6 Identification of outliers by applying Tukey's fences to  $\log(SP_j)$ .
- 7 Removal of outliers from the set of the time segments.
- 8 Repeat steps 5 – 7 until no outlier remains.**

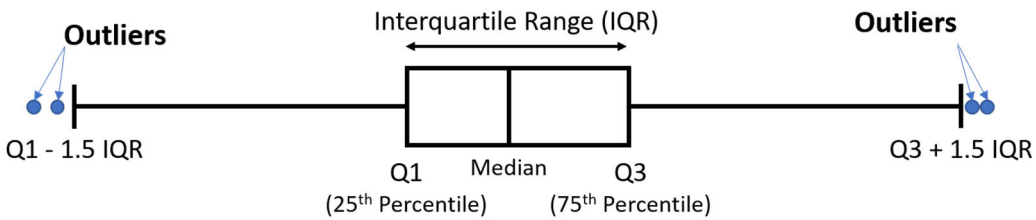


Figure 1. Principle of identification of outlying values using the Tukey's fences on a boxplot.

## 2.2. Calculation of power spectral density (PSD)

In a hypothetic ideal case of the ideally stationary noise, the power spectra estimated from each time segment would be the same and would contain information about the local geological structures. If the ideal stationary noise is weakly disturbed by, e.g., technogenic activities, then the different time segments will have a little bit different power spectra. Statistically, we assume that power spectra of almost stationary noise have a unimodal log-normal distribution. We also assume that the most probable value (the mode) is the best characteristic of the almost stationary noise. Therefore, we can estimate power spectral density of each component as a mode of statistical distribution of power spectra of all  $N_S$  selected time segments. Let  $\mu_C$  be an expected value (mean) and  $\sigma_C$  a standard deviation of logarithm of power spectra:

$$\begin{aligned} \mu_C(f) &= \frac{1}{N_S} \sum_{j=1}^{N_S} \ln \left( \left| \tilde{X}_j^C(f) \right|^2 \right); \\ \sigma_C(f) &= \sqrt{\frac{1}{N_S-1} \sum_{j=1}^{N_S} \left[ \ln \left( \left| \tilde{X}_j^C(f) \right|^2 \right) - \mu_C(f) \right]^2}; \quad C \in \{E, N, Z\} \end{aligned} \quad (5)$$

Then the mode is estimated as

$$PSD_C(f) = \exp \left[ \mu_C(f) - \sigma_C^2(f) \right] \quad (6)$$

From standard deviation of logarithm of power spectra  $\sigma_C$  we can estimate the coefficient of variation as

$$CV_C(f) = \sqrt{\exp \left[ \sigma_C^2(f) \right] - 1} \quad (7)$$

This coefficient quantifies the “spread” of  $PSDs$  and does not depend on the mean or mode value. It quantifies the differences between the time segments at given measurement point regardless of the absolute value of  $PSDs$ . Using coefficient of variation we can estimate “signal-to-noise” ratio (in decibels) as

$$SNR_C(f) = -20 \ln CV_C(f) \quad (8)$$

The “signal” here means the value of  $PSD(f)$  corresponding to the ideal (stationary) noise and the “noise” represents disturbances of the ideal noise due to other sources (e.g., technogenic activity).

Further we will use just a geometric average of horizontal components instead of two individual horizontal components

$$PSD_H(f) = \sqrt{PSD_E(f) PSD_N(f)} \quad (9)$$

where  $E$  and  $N$  indicate the EW and NS components, respectively, and  $H$  the geometrical average. The standard deviation and  $SNR$  of the averaged horizontal component are

$$\sigma_H(f) = \sqrt{\sigma_N^2(f) + \sigma_E^2(f)} \quad SNR_H(f) = -10 \ln \left[ \exp \left( \sigma_H^2(f) \right) - 1 \right] \quad (10)$$

Having computed  $PSD_C(f); C \in \{H, Z\}$ , we can also evaluate their ratio, standard deviation and  $SNR$  as

$$\begin{aligned} PSD_{H/Z}(f) &= \frac{PSD_H(f)}{PSD_Z(f)} \\ \sigma_{H/Z}(f) &= \sqrt{\sigma_H^2(f) + \sigma_Z^2(f)} \quad SNR_{H/Z}(f) = -10 \ln \left[ \exp \left( \sigma_{H/Z}^2(f) \right) - 1 \right] \end{aligned} \quad (11)$$

$PSD_{H/Z}(f)$  is similar to the common H/V spectral ratio. The main difference is that we estimate the mode of  $PSDs$  instead of averaging spectra over time segments. Moreover, in the

H/V ratio method, usually the H/V spectral ratios are first evaluated for all time segments and then averaged (Bard et al. 2004). However, as it was shown by Albarello & Lunedei (2013), the H/V ratios computed from averaged horizontal and vertical spectra have smaller biases than the averaged H/V ratios.

Once  $PSD_C(f)$ ;  $C \in \{H, Z, H/Z\}$  are calculated for all measurement points, they may be visualized together in one graph in order to check presence of obvious outliers. The outliers have to be removed from further analysis.

An additional visualisation of  $\sigma_C(f)$  or  $SNR_C(f)$ ;  $C \in \{H, Z, H/Z\}$  helps to identify frequencies with large values of standard deviation which usually mean multimodal distribution, i.e. the nonstationary noise caused by technogenic activity. In such a case the selection based on application of Tukey's fences is not applicable. Such frequencies must be then interpreted with caution or potentially excluded from further analysis.

### 2.3. Introduction of FISPs – the Finite-Interval Spectral Power

Consider a free-surface site with some underground geologic conditions and the corresponding spectrum of noise. The spectrum may have peaks representing local amplification of noise. In case of laterally varying conditions, the peak frequencies can change from receiver to receiver. Inclusion of a cavity (tens of meters in diameter, depth of tens-to-hundreds of meters) will cause appearance of additional, relatively small spectral peaks but at several frequencies. (Several peak frequencies were observed, e.g., by Kolesnikov & Fedin, 2018, and Schneider et al., 2017, in their models.) The presence of spectral peaks due to the cavity and spectral peaks due to surrounding conditions in the spectrum of noise can make it difficult to identify individual spectral peaks caused by the cavity at the sites with complex surrounding conditions.

Therefore, it is reasonable to expect that the methods based on the identification of individual spectral peaks related to cavity will face problems mainly in detecting deeper cavities in complex geologic conditions. An example of the spectral analysis of noise based on identification of individual peaks is the frequently used H/V ratio method (e.g., Bard et al. 2004, Bonnefoy-Claudet et al. 2006) for the estimation of fundamental resonance frequency in site effects studies.

Instead of problematic identification of individual weak peaks and calculation of corresponding spectral characteristics, it might be advantageous to use a spectral characteristic comprising a finite-interval of frequencies. Moreover, in practice it is easier to select an interval of frequencies where effects of cavity can be expected than to reliably relate an individual peak

with the cavity. As it was shown by Kristek et al. (2019) and Kristekova et al. (2019) based on the 3D numerical simulations of noise (Moczo & Kristek, 2002), the spectral power can be used for visualizing spatial variations of subtle changes of spectral content of noise. Therefore, we propose to evaluate spectral power in a reasonably selected frequency interval. We define the finite-interval spectral power (*FISP*) as

$$FISP_j^H = \int_{F_{\min}}^{F_{\max}} |\tilde{X}_j^E(f)| |\tilde{X}_j^N(f)| df, \quad FISP_j^Z = \int_{F_{\min}}^{F_{\max}} |\tilde{X}_j^Z(f)|^2 df \quad (12)$$

Because we assume that *FISPs* have a unimodal log-normal distribution, we can estimate the most probable value (the mode) using equations similar to eqs. (5) - (8)

$$\begin{aligned} \mu_C^{FISP} &= \frac{1}{N_S} \sum_{j=1}^{N_S} \ln(FISP_j^C) \\ \sigma_C^{FISP} &= \sqrt{\frac{1}{N_S-1} \sum_{j=1}^{N_S} [\ln(FISP_j^C) - \mu_C^{FISP}]^2} \\ FISP_C &= \exp \left[ \mu_C^{FISP} - (\sigma_C^{FISP})^2 \right] \\ CV_C^{FISP} &= \sqrt{\exp \left[ (\sigma_C^{FISP})^2 \right] - 1} \\ SNR_C^{FISP} &= -20 \ln CV_C^{FISP}; \quad C \in \{H, Z\} \end{aligned} \quad (13)$$

Once we have *FISPs* evaluated for all measurement points and both components, we can construct aerial maps covering the measurement area.

Obviously, the question is how to determine values of  $F_{\min}$  and  $F_{\max}$  in order to obtain anomalous values of *FISP* above the cavity. Very small values of  $F_{\min}$  would potentially lead to including effects of medium much larger than the cavity. Too large value of  $F_{\max}$  could potentially lead to sensitivity to heterogeneities significantly smaller than the cavity. If the size of the cavity is unknown, *FISP* should be evaluated for several trial values of  $F_{\min}$  and  $F_{\max}$ . The choice of  $F_{\min}$  and  $F_{\max}$  should eliminate the lower and higher frequencies at which differences among *PSDs* for individual stations considerably increase with decreasing and increasing frequencies, respectively. In Section 3.3 we describe how we applied this procedure to the Felsőpetén data.

In addition to the  $FISP_H$  and  $FISP_Z$  it also useful to evaluate and map their ratio  $FISP_H / FISP_Z$ . Because both  $FISP_H$  and  $FISP_Z$  have log-normal distribution, their ratio will have also log-normal distribution. Therefore, their ratio could be estimated as

$$\begin{aligned}\mu_{H/Z}^{FISP} &= \frac{1}{N_S} \sum_{j=1}^{N_S} \ln \left( \frac{FISP_j^H}{FISP_j^Z} \right) \\ \sigma_{H/Z}^{FISP} &= \frac{1}{N_S - 1} \sqrt{\sum_{j=1}^{N_S} \left[ \ln \left( \frac{FISP_j^H}{FISP_j^Z} \right) - \mu_{H/Z}^{FISP} \right]^2} \\ FISP_{H/Z} &= \exp \left[ \mu_{H/Z}^{FISP} - (\sigma_{H/Z}^{FISP})^2 \right] \\ CV_{H/Z}^{FISP} &= \sqrt{\exp \left[ (\sigma_{H/Z}^{FISP})^2 \right] - 1} \\ SNR_{H/Z}^{FISP} &= -20 \ln CV_{H/Z}^{FISP}\end{aligned}\quad (14)$$

## 2.4. Interpretation of the FISP maps and testing cavity location with respect to configuration of measurement points

A position of the cavity should be visible at least on one of the maps showing  $FISP_H$ ,  $FISP_Z$  and  $FISP_{H/Z}$  as an anomalous pattern with approximately azimuthal symmetry. The centre of the pattern should correspond to the horizontal position of centre of the cavity. In case of a shallow horizontally elongated cavity the pattern can be elongated as well.

Because the anomalous value of  $FISP$  can be, in principle, due to spectral amplification at just one frequency (e.g., due to a monochromatic source near or at the measurement point it is reasonable to check  $PSD_C ; C \in \{H, Z\}$  as a function of frequency along profiles of measurement points crossing the position of the  $FISP$  anomaly. Along the profiles we should see amplification in a range of frequencies. This will be illustrated in the next section.

If the distribution of the measurement points is not too sparse, removal of a station nearest to the centre of the cavity can weaken, however not completely remove, the identifying anomalous pattern. Therefore, it is reasonable to plot  $FISP$  maps and  $PSD_C ; C \in \{H, Z\}$  along profiles without including that station.

### 3 Application to the Felsőpetény, Hungary, CTBTO data

As already mentioned, the detection of cavities due to underground nuclear explosions is a primary task for a CTBT OSI. For this, capable methods for analysing data derived from measurements of noise and potentially also earthquakes during a limited period of time after a suspected underground nuclear explosion are important. Obviously, methods based on analysis of noise are more important because we cannot rely on a sufficient number of earthquakes.

#### 3.1. The Field Test in Felsőpetény (Hungary)

The team of experts participating at the field test performed extensive geophysical measurements in the area near the small village of Felsőpetény, Hungary, in 2019 (Fig. 2). The reason for selecting this site was a known oval cavern with a horizontal diameter of 28-30 m, height of 25-28 m, and ceiling located approximately 70 m below the free surface. The goal of the active and passive experiments was to develop a geotechnical model of the site and to investigate the effect of the cavern on the measured geophysical fields. The analyses of the acquired data are still ongoing.

We were provided with continuous records of noise at 50 measurement points in the area of interest (Fig. 2). The area (approximately 400 m x 450 m) covered by the measurement points is approximately centred at the horizontal position of the cavern. The interstation distance is approximately 50 m. We assume that the size of the area is sufficient with respect to the size and depth of the cavern.

Noise was recorded continuously for almost 7 days, September 11-18, 2019. Thus, the records include noise during days and nights, workdays and holidays. Lennartz LE3D light seismometers were used and the sampling frequency was 500 Hz. The usable data are in the frequency range [0.5, 80] Hz.

An illustration of the seismic records (Fig. 3(a)) shows a continuous 24h record at the measurement point 4003. Transients and day-night variation of noise are clearly visible, though it was Saturday.

#### 3.2. Tukey's fences applied to spectral power

Fig. 3(a) shows that the record even during the Saturday is very much distorted by strong transients. It is therefore reasonable to select a sufficiently long window of the night (less distorted) record. We selected a 6h window from 8h pm (Sunday) as a suitable window for all measurement points. The selected window is shown in Fig. 4(a).

We divided the 6h window into 863 50-second segments and calculated value of  $SP$  for each segment. The values of  $SP$  for the measurement point 4003 are shown in Fig. 4(b). (Just for illustration, in Fig. 3(b) we show  $SP$  values for 3455 segments of the whole 24h record.) The red lines in Figs. 3(b) and 4(b) correspond to Tukey's fences. Segments with  $SP$  values outside the Tukey's fences are considered outliers and are eliminated from further analysis. We clearly see that in case of very much distorted noise (Fig. 3), the spectral power does not have a unimodal log-normal distribution, hence the Tukey's fences are not applicable directly to the whole record.

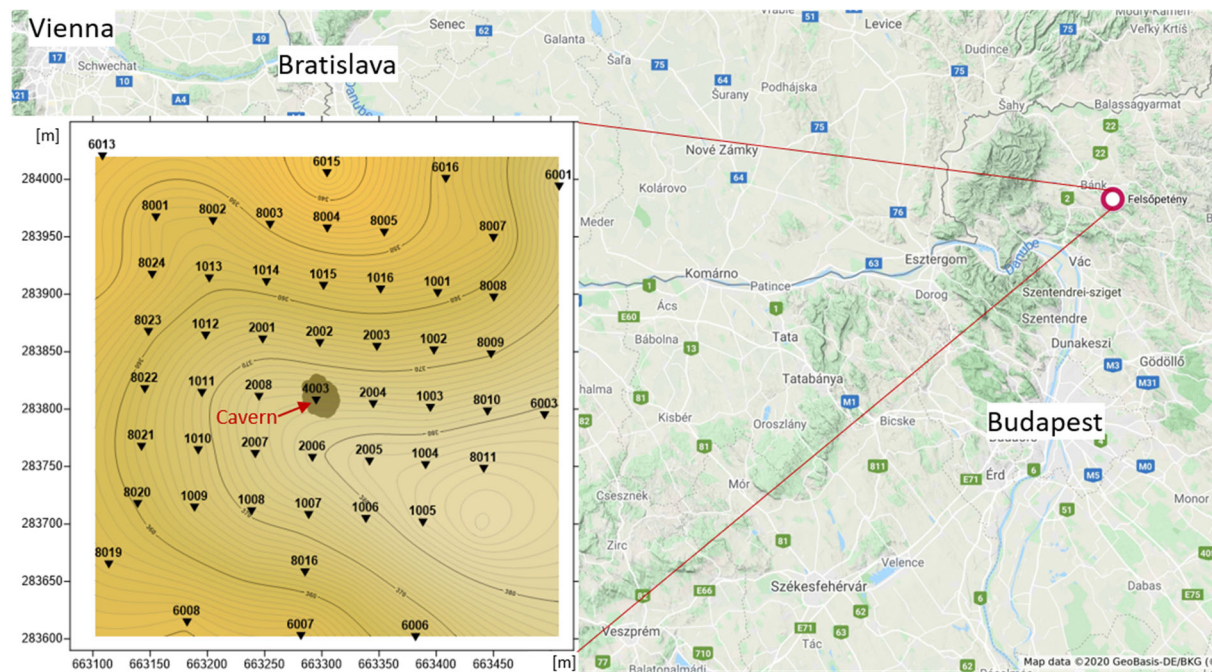


Figure 2. Location of the Felsőpetény (Hungary) Field Test (FT2019), location of the cavern and positions of the measurement points shown in the topographic map. Numbers in the map indicate elevation.

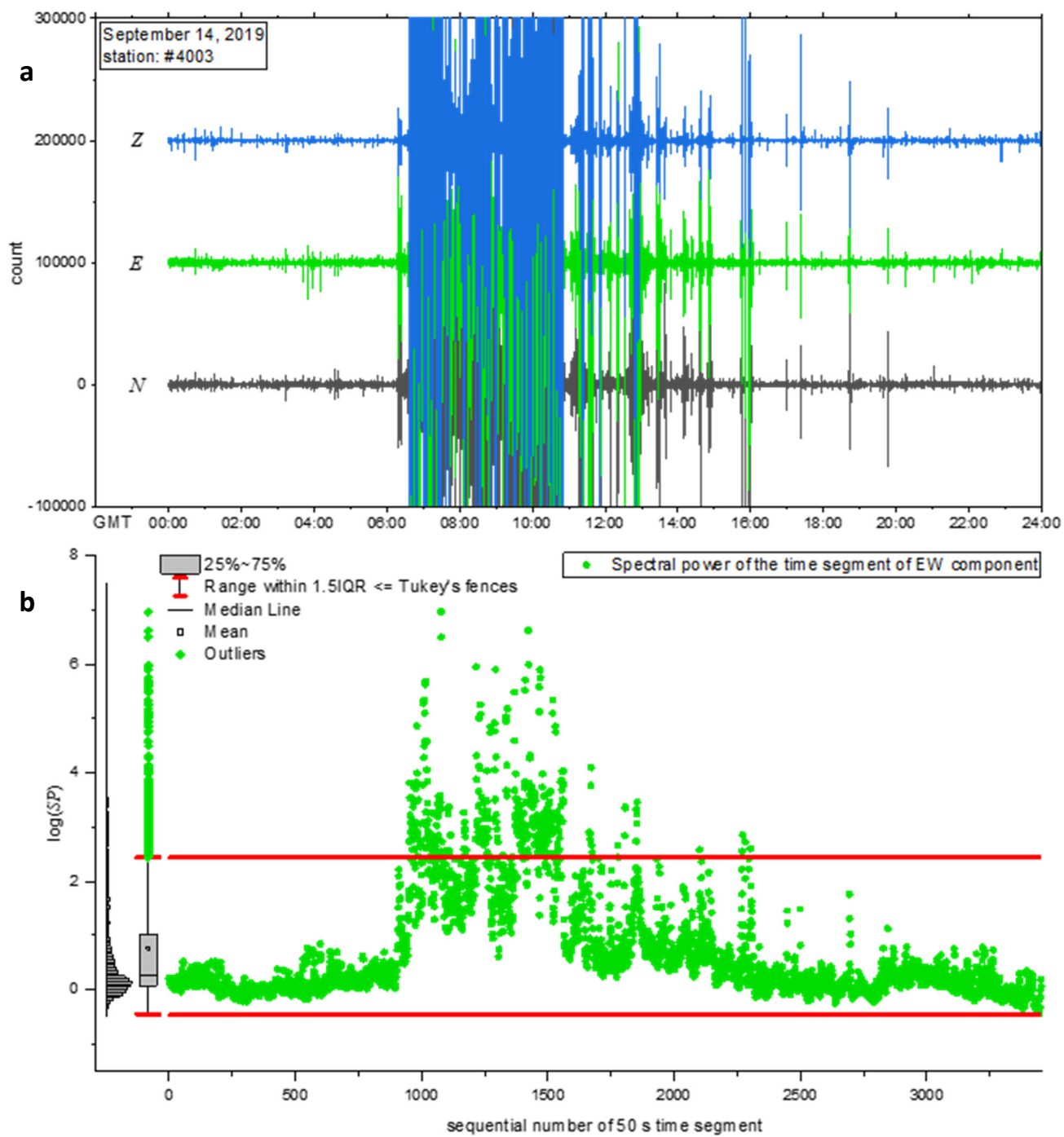


Figure 3. (a) The continuous 24h record of the EW, NS and vertical components of the particle velocity recorded at the measurement point 4003. The large amplitudes are clipped. (b) Values of the spectral power evaluated for each of 3455 segments of the 24h record.

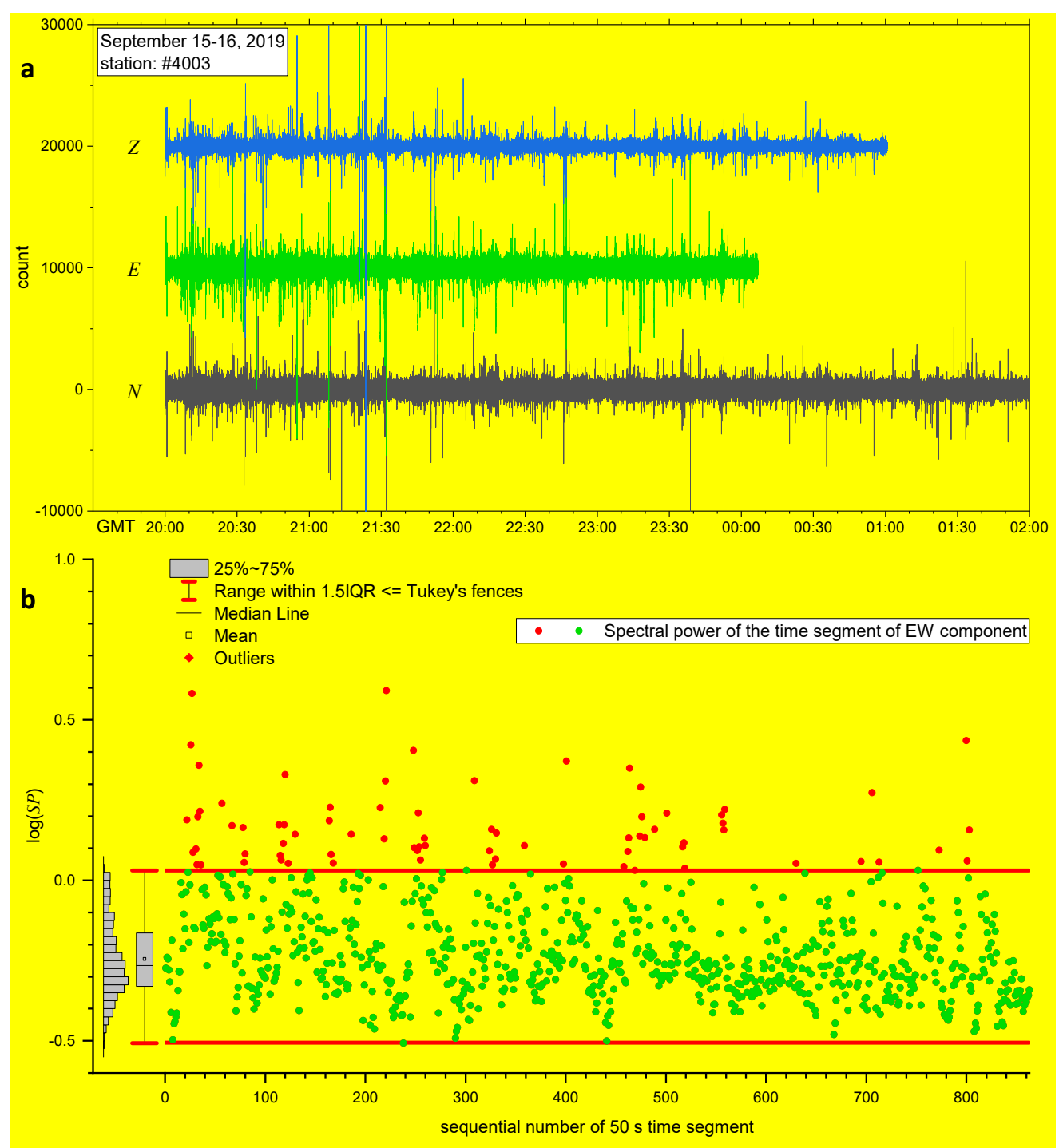


Figure 4. (a) The 6h window selected for further analysis. (b) Values of the spectral power evaluated for each of 863 segments of the 6h window.

### 3.3. Power Spectral Densities (PSD) for all measurement points

Fig. 5 shows the horizontal and vertical *PSDs* as well as the horizontal-to-vertical *PSDs* ratio for all measurement points in the left panel and corresponding *SNRs* in the right panel. There are 3 obvious outliers (measurement points 6013, 8005 and 8023) that were eliminated from further analysis. *PSDs* above 30 Hz are more scattered than those inside the interval [1, 30] Hz. This is also visible on lower values of *SNRs* above 30 Hz. *PSDs* at higher frequencies are likely considerably affected by heterogeneities smaller than the cavity. Looking at frequencies less than 30 Hz we can see that in the interval [approx. 5, 30] Hz there are several curves that differ from majority. This could be the potential effect of cavity. *PSDs* below 5 Hz could be more affected by medium much larger than the cavity. Also, the *SNRs* in the interval [approx. 5, 30] Hz have the largest values, despite the distinct and sharp minimum at 5 Hz. We have found out that at almost all measurement points there are several time segments with much lower amplitudes at 5 Hz than in other time segments. Such sudden disappearance of energy at 5 Hz at all measurement points at the same time strongly indicates technogenic origin of peak at 5 Hz. Therefore, the frequency interval for calculating *FISPs* should not include 5 Hz. We selected [5.5, 30] Hz. Obviously, the selection of the frequency interval is approximate and based on visual evaluation of *PSDs* and *SNRs*. Therefore, *FISPs* should be always calculated and checked also for other frequency interval(s). We calculated *FISPs* also for a wider interval [2, 30] Hz.

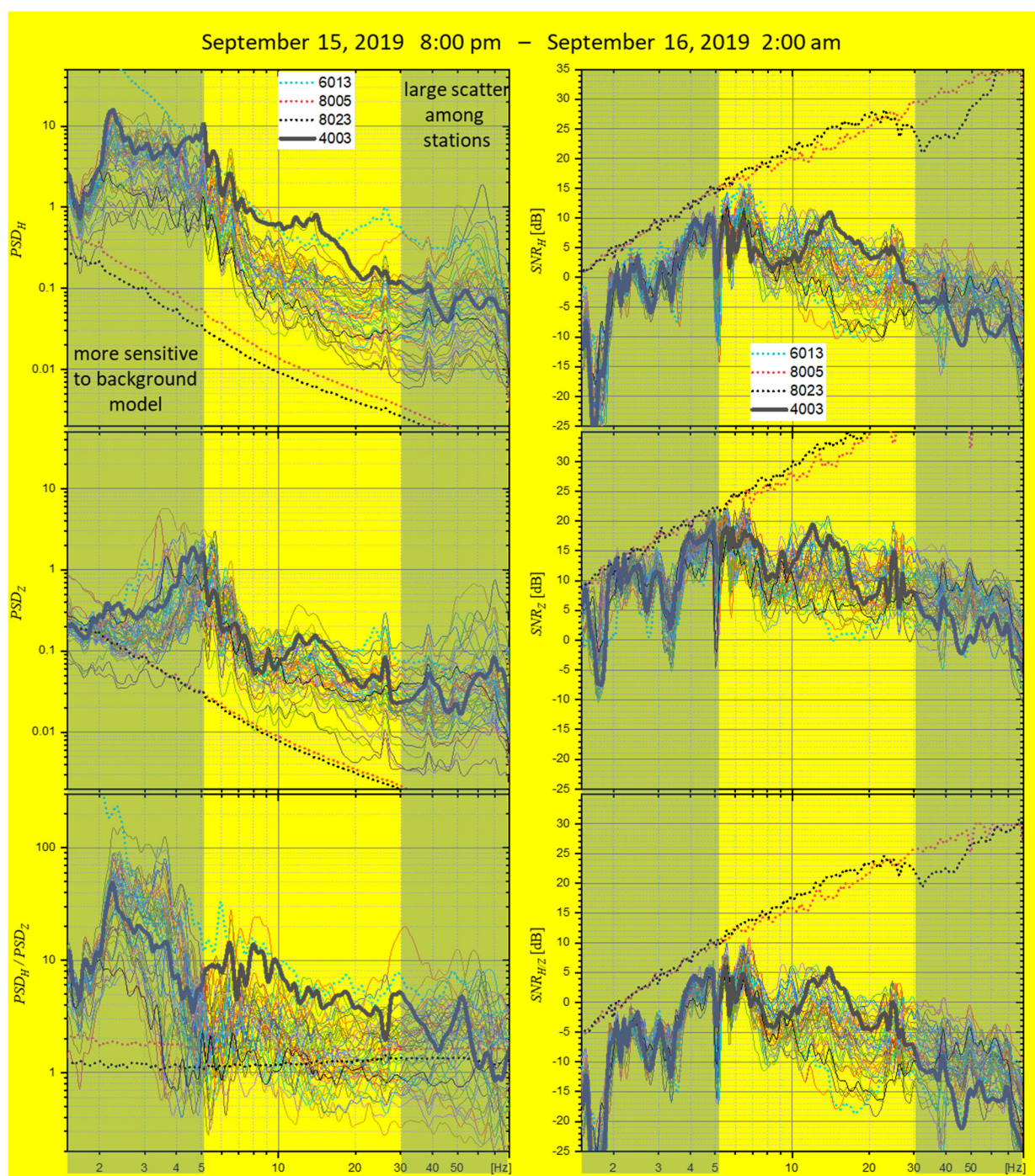


Figure 5. Horizontal  $PSD_H$ , vertical  $PSD_Z$ , and their ratio  $PSD_H / PSD_Z$  for all measurement points (left panel) and corresponding  $SNRs$  (right panel). Three obvious outliers (measurement points 6013, 8005 and 8023) were eliminated from the further analysis. The measurement point 4003 just above the cavity is highlighted. We first calculated *FISPs* for the frequency interval [5.5, 30] Hz.

### 3.4. FISP maps

Once we have *FISPs* evaluated for all measurement points, we can construct aerial maps covering the measurement area. Fig. 6 shows aerial maps of  $FISP_H$ ,  $FISP_Z$  and  $FISP_{H/Z}$  for two frequency intervals. We clearly recognize localized anomalous pattern in maps of  $FISP_H$  and  $FISP_{H/Z}$ . The centre of the anomalous pattern in the frequency interval [5.5, 30] Hz agrees with the horizontal position of centre of the cavern. In case of the frequency interval [2, 30] Hz the centre is shifted approximately 60 m to SE. As we mentioned earlier, the visual evaluation of *PSDs* and *SNRs* for all measurement points led us to prefer frequency interval [5.5, 30] Hz because inclusion of lower frequencies considerably enhances effect of the medium much larger than the cavern and thus potentially decreases accuracy of location.

Fig. 7 shows aerial maps of  $SNR_H^{FISP}$ ,  $SNR_Z^{FISP}$  and  $SNR_{H/Z}^{FISP}$  for two frequency intervals.

Here we assume 10 dB as the threshold level (depicted by the black line). Values of *SNRs* higher than 10 dB indicate more robust (reliable) value of *FISP*. Therefore, we choose the green colour in aerial maps for values larger than 10 dB. The values of *SNR* smaller than 10 dB indicate that corresponding *FISP* values should be interpreted with caution. Therefore, we choose red colour in aerial maps for these values. Note that selection of the threshold value could be case dependent. Let us recall that  $FISP_{H/Z}$  is computed from the ratio of  $FISP_H$  and  $FISP_Z$  at each time segment and therefore the aerial maps of  $SNR_{H/Z}^{FISP}$  could have different patterns and values than  $SNR_H^{FISP}$  or  $SNR_Z^{FISP}$ .

We cannot explain why the anomalous pattern is not visible in the maps of  $FISP_Z$ . We do not see the possibility to explain this based on the available data. We think that appearance of an anomalous patterns on the vertical and horizontal components may differ case to case depending on the geometry and depth of cavity, structural parameters and sources of noise.

### 3.5. Power Spectral Densities along profiles of measurement points crossing the position of the FISP anomaly

As we explained earlier, it is necessary to check whether the anomalous values of *FISPs* are not due to amplification at just one frequency corresponding, e.g., to a monochromatic source near or at a measurement point. It is therefore important to see *PSDs* as a function of frequency. This is possible along profiles of measurement points crossing the position of the centre of the anomaly.

1  
2 Fig. 8 shows  $PSD_H$ s along the NS, NE-SW, WE and NW-SE profiles of measurement  
3 points. We can see a systematic pattern in the plots of  $PSD_H$ s along all depicted profiles:  
4  $PSD_H$  attains large values just at the horizontal position of the centre of the cavern in the  
5 frequency interval [5.5, 30] Hz. There are comparably large values of  $PSD_H$  close to the NW  
6 end of the NW-SE profile. The corresponding measurement point is, however, at the border of  
7 the covered area and closest to the measurement point 6013 which had to be eliminated from  
8 the analysis because the  $PSD_H$  was a clear outlier in the graph showing  $PSD_H$ s for all  
9 measurement points – see Fig. 5.  
10  
11  
12  
13  
14  
15  
16  
17

18 We conclude that the  $PSD_H$ s along the NS, NE-SW, WE and NW-SE profiles of  
19 measurement points confirm the horizontal position of centre of the cavern indicated in the  
20 aerial maps of  $FISP_H$ ,  $FISP_Z$  and  $FISP_{H/Z}$  – see Fig. 6.  
21  
22  
23  
24  
25  
26  
27  
28  
29  
30  
31  
32  
33  
34  
35  
36  
37  
38  
39  
40  
41  
42  
43  
44  
45  
46  
47  
48  
49  
50  
51  
52  
53  
54  
55  
56  
57  
58  
59  
60

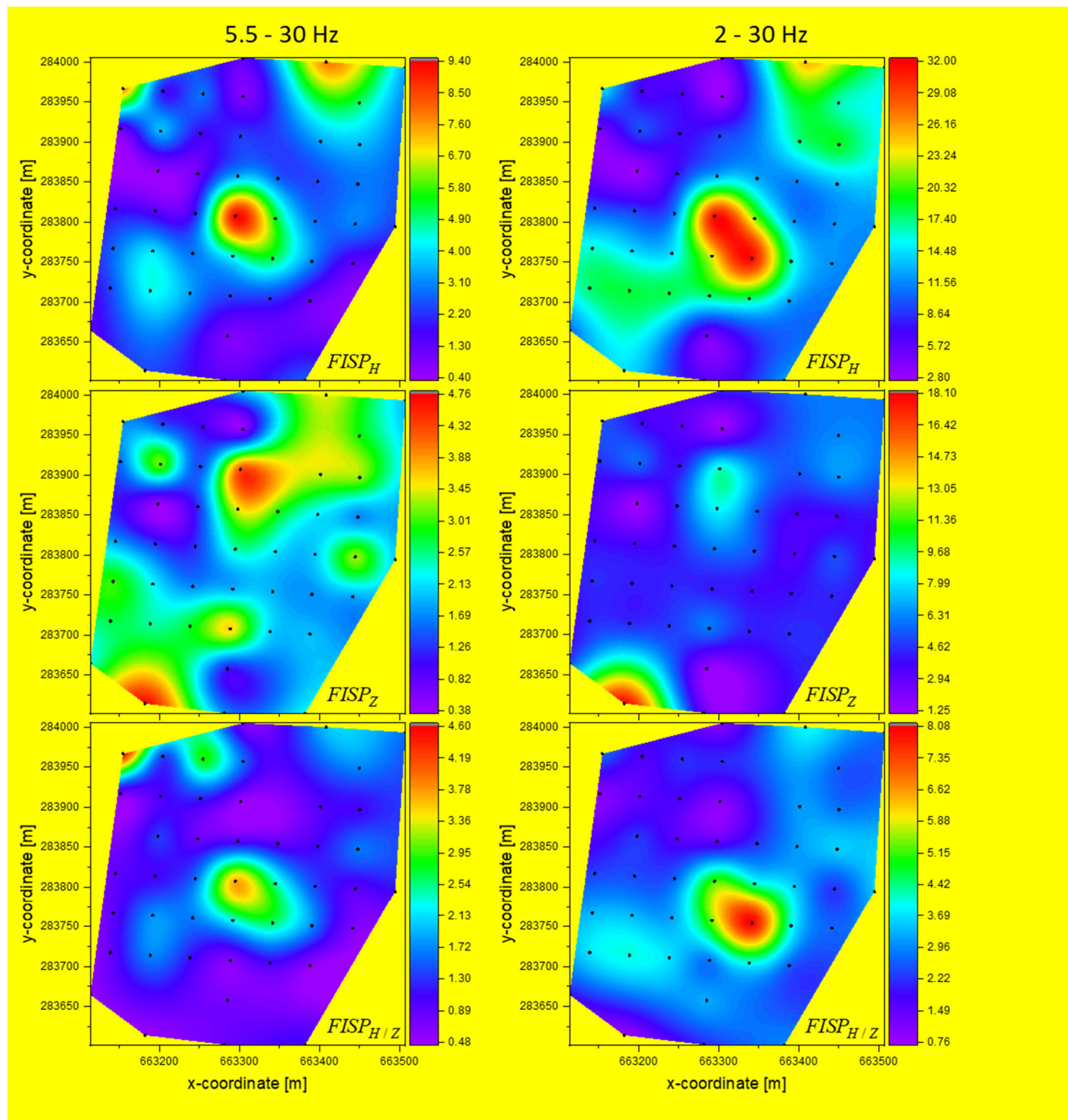


Figure 6. Aerial maps of  $FISP_H$ ,  $FISP_Z$  and  $FISP_{H/Z}$  for two frequency intervals.

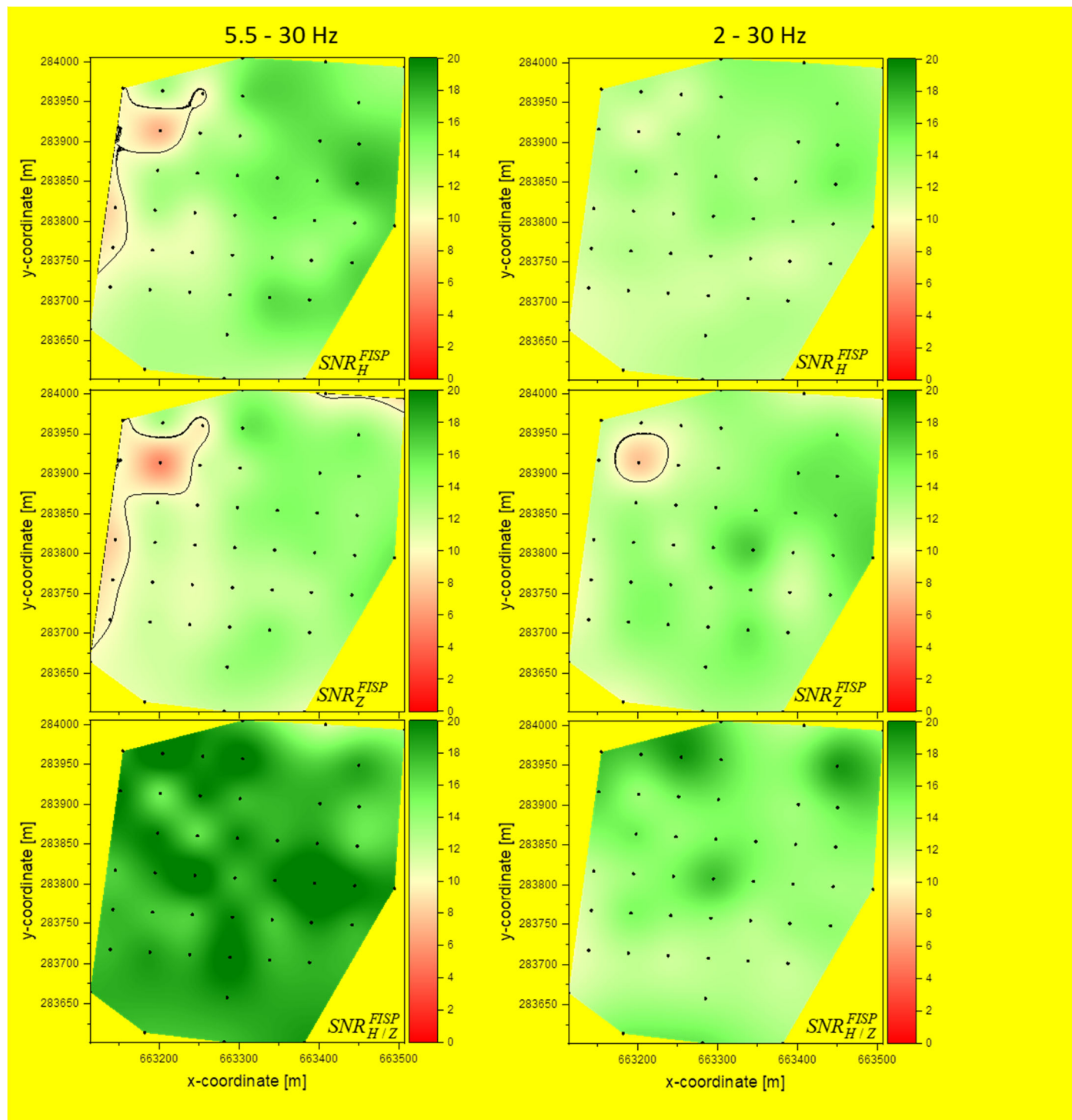


Figure 7. Aerial maps of  $SNR_H^{FISP}$ ,  $SNR_Z^{FISP}$  and  $SNR_{H/Z}^{FISP}$  for two frequency intervals.

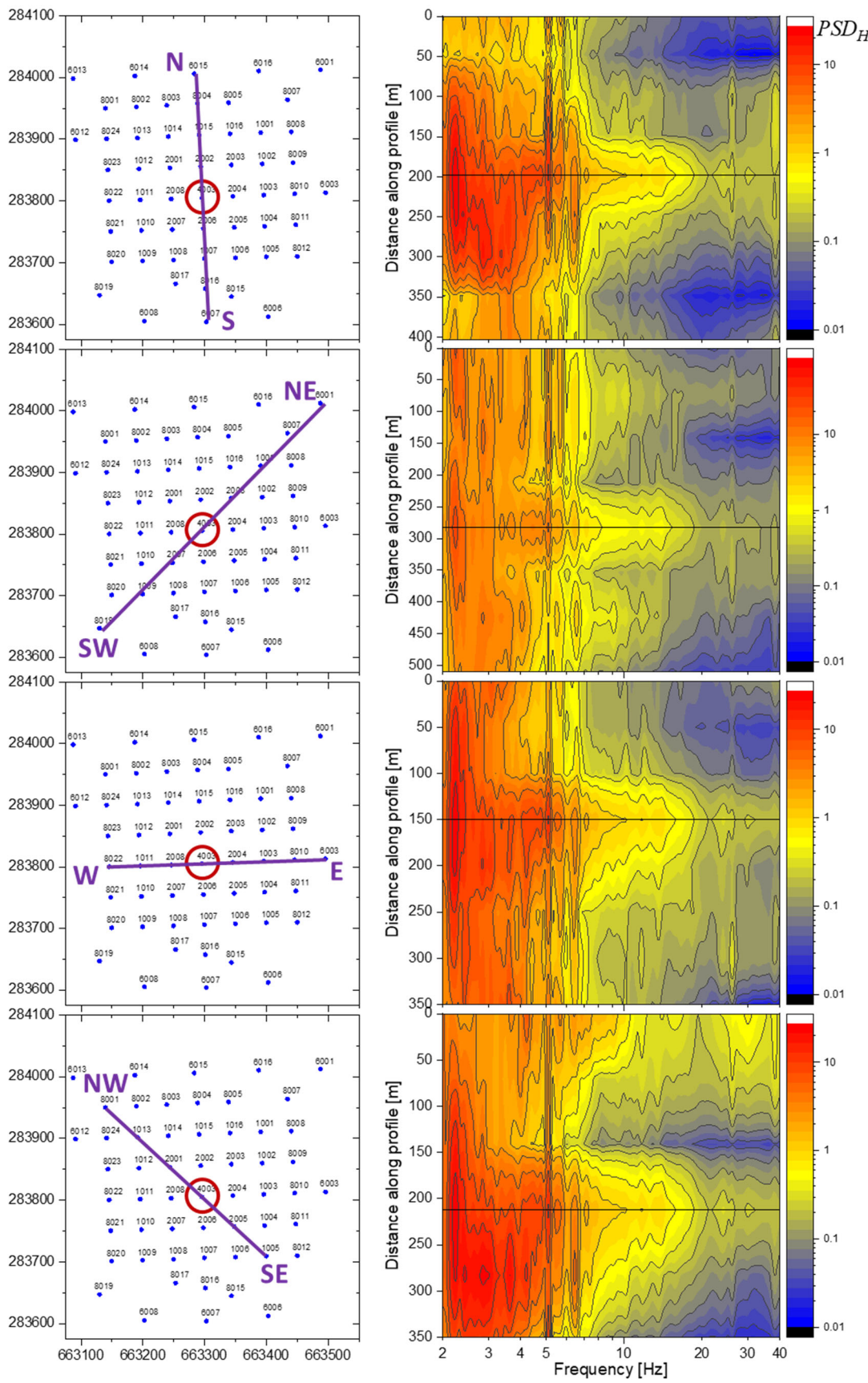


Figure 8. Power spectral density of the horizontal component  $PSD_H$  as a function of frequency and position along the NS, NE-SW, WE and NW-SE profiles of measurement points. Position of the cavern is indicated by the red circle on the profiles and by the horizontal red line in the  $PSD_H$  plots.

## 4 DISCUSSION

Considering the size of the cavern and distribution of the measurement points shown in Fig. 2, we may intuitively guess that the density of the measurement points is at the threshold level. Therefore, it is interesting to check the aerial maps of  $FISP_H$ ,  $FISP_Z$  and  $FISP_{H/Z}$  from which the contribution of the measurement point 4003 (just above the cavern) is removed. Fig. 9 shows aerial maps of  $FISP_H$ ,  $FISP_Z$  and  $FISP_{H/Z}$  in the frequency interval [5.5,30] Hz for all measurement points (left panel) and for all measurement points except point 4003 (right panel). We can see that the anomaly at  $FISP_H$ , and  $FISP_{H/Z}$  above the cavity is not due to a single measurement point. This is well seen on the map showing  $FISP_{H/Z}$  without measurement point 4003 although the largest value on the map is at the point 8001 (top left corner). Just the point 8001 is an example of a single point causing anomaly. If we remove the point 8001, the resulting map will be dominated by the anomaly above cavity – with or without including point 4003.

If the anomalous pattern was not visible in the map without contribution by point 4003, it would be an indication that the distribution of the measurement points should be denser. In practice, because we do not assume an array with simultaneous measurement, it would be enough to perform additional single-station measurements in the subarea indicated by the anomalous pattern. Clearly, the simple possibility to increase the number of measurement points is the advantage of our method.

In order to test the possibility of increasing the number of measurement points by additional (single-station) measurements, we selected another 6h time window between Monday 7 pm and 1am Tuesday. Fig. 10 shows horizontal, vertical and horizontal-to-vertical ratio PSDs for all measurement points (left panel) and their SNRs (right panel) for 6h time window. There are still 3 obvious outliers (measurement points 6013, 8005 and 8023). Comparing with Fig. 5 (Sunday's time window) we can see that the horizontal components have smaller spectral amplitudes at almost all frequencies whereas the vertical components are not so much different. Therefore, also  $PSD_{H/Z}$  have smaller values in the Monday's time window than in the Sunday's. This indicate that the noise conditions were different during the two 6h time windows. If we want to mix data from these different time windows, i.e., take some measurement points from the first window and some points from the second window into one FISP analysis, it is necessary to “rescale” the PSDs from the second window according to the PSDs from the first window. This, however, requires having at least one common measurement point in both time windows. The common point can be then used for estimating

a rescale function. Fig. 11 shows aerial maps of  $FISP_H$ ,  $FISP_Z$  and  $FISP_{H/Z}$  (left panel) and  $SNR_H^{FISP}$ ,  $SNR_Z^{FISP}$  and  $SNR_{H/Z}^{FISP}$  (right panel) for data obtained by mixing the two time windows. Black points indicate Sunday's data, yellow points indicate Monday's data. The measurement point 1003 (in red) was taken as the common point because, as it is clear from Fig. 7, it has a very high value of  $SNR_{H/Z}^{FISP}$ . By comparing Figs. 6 and 11 we see that by mixing data from the two 6h time windows we obtained very similar patterns in  $FISP$  aerial maps. Fig. 11 shows that  $SNRs$  in the Monday's data (yellow measurement points) have smaller values due to more distorted noise. These smaller values, however, only slightly affected the resulting pattern of  $FISPs$  in the composite  $FISP$  map.

The surrounding medium around the cavern cannot be considered as structurally simple, e.g. as a homogeneous block of material. The structural complexity is due to both natural reasons (karst region) and mining activity. Therefore, the distinctive anomalous pattern seen in the aerial maps of  $FISP_H$ ,  $FISP_Z$  and  $FISP_{H/Z}$  can be considered as encouraging for using the method, and further testing its applicability and limits in various configurations.

Clearly, the considerably more heterogeneous surrounding medium could lead to aerial maps with more complex  $FISP$  distributions. If, in such a case, more measurement points would not lead to one distinctive anomalous pattern, some additional data might be necessary for locating an underground cavity.

Considering potential structural complexity of the underground medium and complexity of the noise itself, we certainly cannot conclude now what is the potential of the presented approach to be a standalone method for identifying underground cavity. In any case, the method can be useful as a companion to other independent methods.

It is obviously reasonable to perform an additional parametric investigation based on extensive numerical simulations of seismic ambient noise for a representative variety of underground configurations. If sufficiently realistic, such a study may provide some insights into the method capabilities. We will explore this possibility in the separate study.

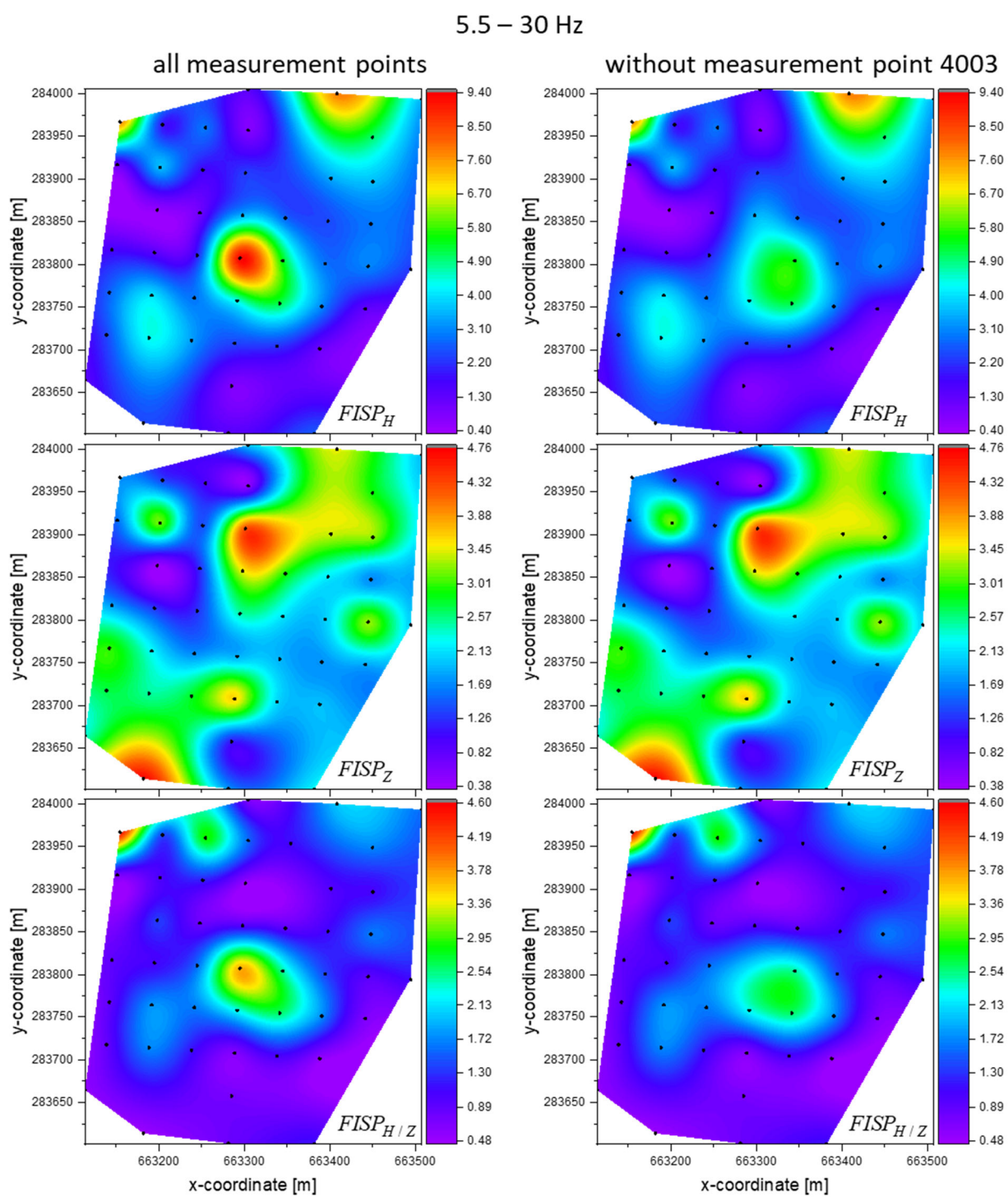


Figure 9. Aerial maps of  $FISP_H$ ,  $FISP_Z$  and  $FISP_{H/Z}$  in the frequency interval [5.5,30] Hz for all measurement points (left panel) and for all measurement points except point 4003 (right panel).

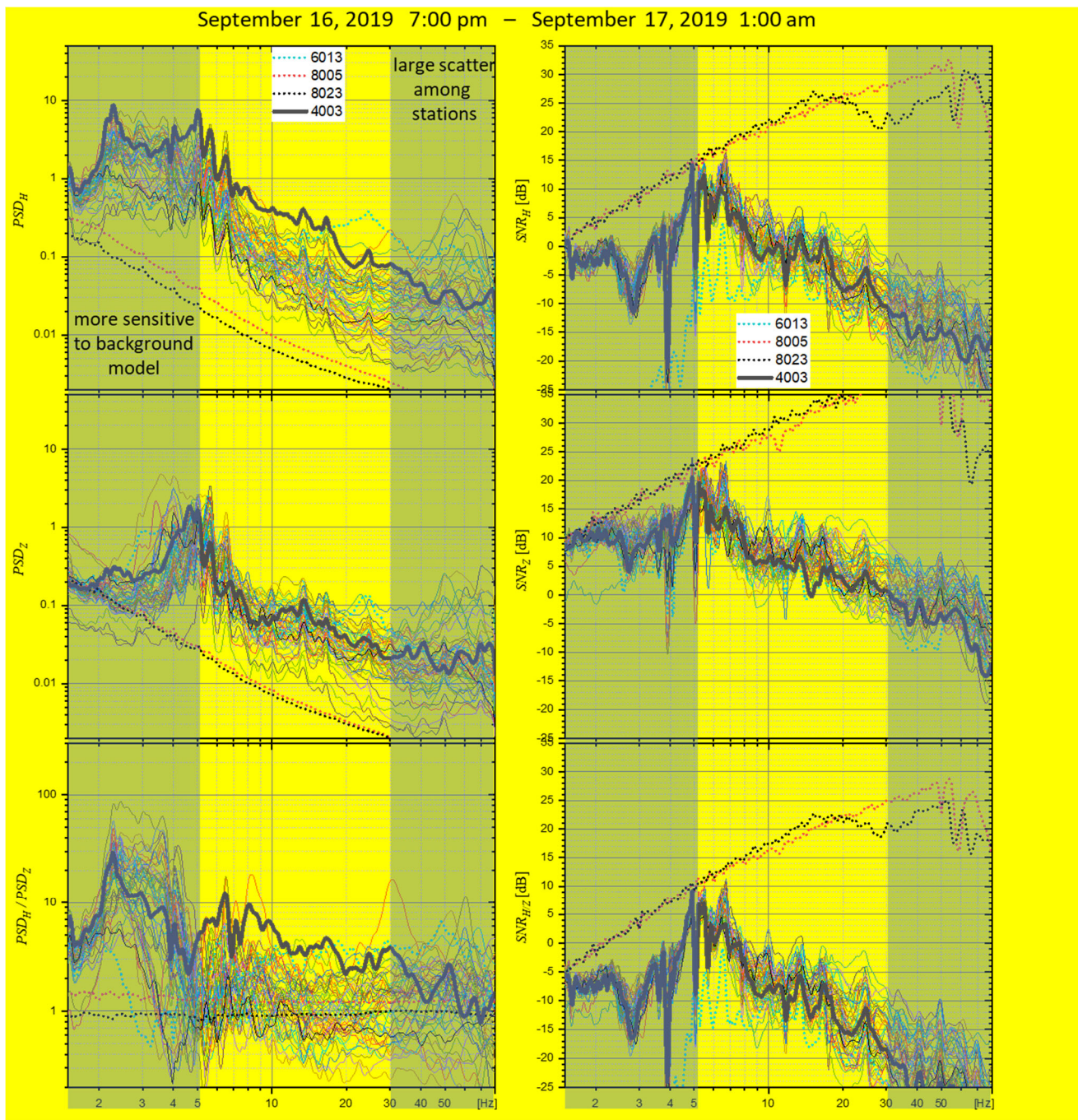


Figure 10. Horizontal  $PSD_H$ , vertical  $PSD_Z$ , and their ratio  $PSD_H / PSD_Z$  for all measurement points (left panel) and corresponding  $SNRs$  (right panel) for Monday's 6h time window. Three obvious outliers (measurement point 6013, 8005 and 8023) were eliminated from the further analysis. The measurement point 4003 just above the cavity is highlighted.

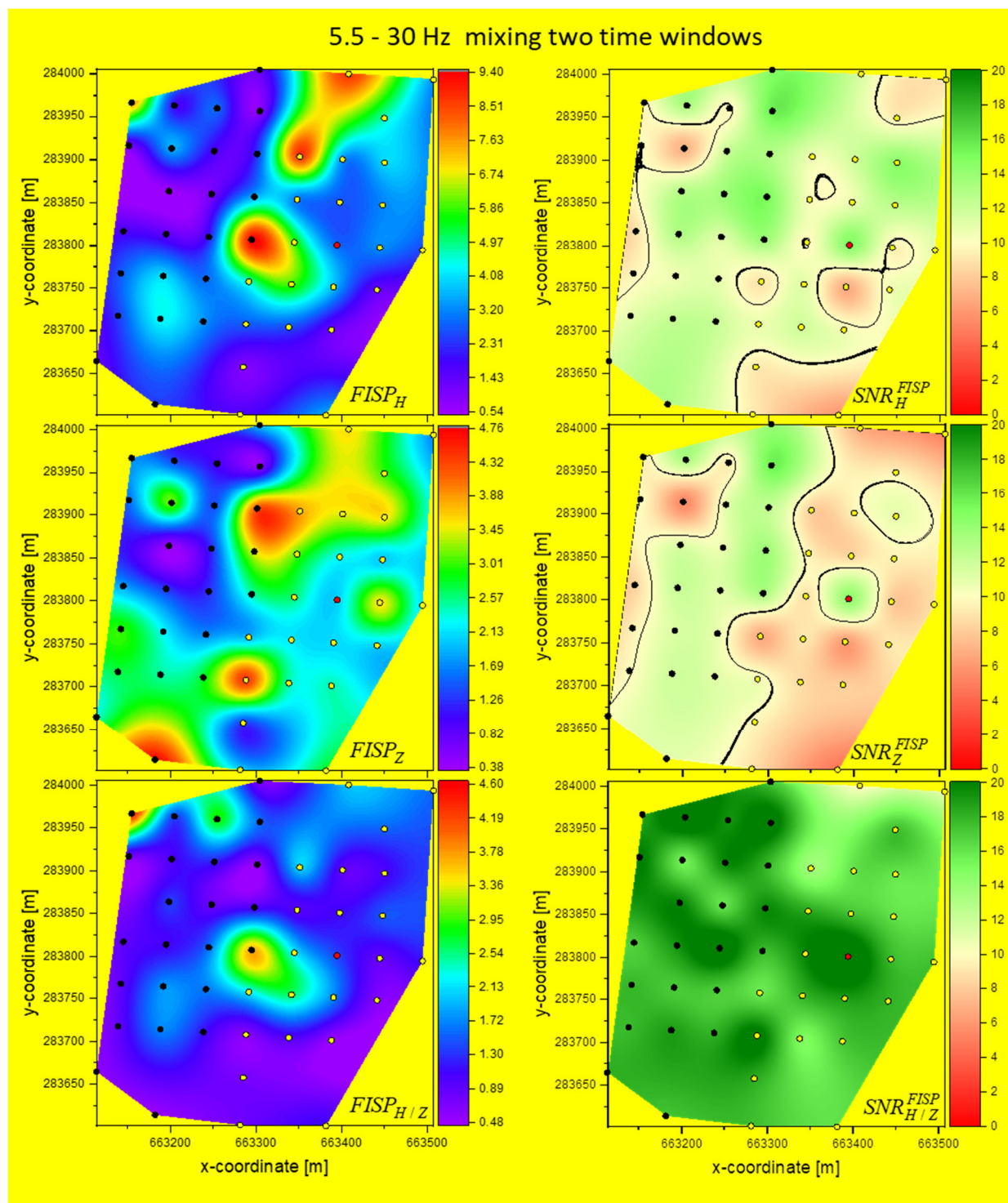


Figure 11. Aerial maps of  $FISP_H$ ,  $FISP_Z$  and  $FISP_{H/Z}$  (left panel) and  $SNR_H^{FISP}$ ,  $SNR_Z^{FISP}$  and  $SNR_{H/Z}^{FISP}$  (right panel) for data obtained by mixing two time windows for which PSDs are shown in Figs. 5 and 10. In black – measurement points for Sunday's data, in yellow – measurement points for Monday's data. The measurement point 1003 (in red) was taken as the common point.

## 5 CONCLUSIONS

We present a new method which uses the Finite-interval Spectral Power (FISP) of seismic ambient noise for detecting and locating a horizontal position of underground cavity. The application of the method in practice is simple because it makes it possible to use single-station measurements. The method assumes

- a set of potentially irregularly distributed measurement points in the area on the Earth's free surface over a suspected cavity,
- sufficiently long 3-component records of seismic ambient noise at all measurement points.

The records should be obtained in similar conditions, however, the measurements may be performed sequentially. In such a case it is advisable to have one fixed measurement point at which the noise would be recorded simultaneously with recording at any other measurement point. This would make it possible to align noise levels from different measurements.

We also present a method of automatic identification of time segments in the records of seismic ambient noise which are distorted and thus not usable for evaluating a desired characteristic(s) of the noise. This method can be used in any seismic ambient noise analysis requiring time segments of stationary noise.

We tested applicability of the method using records of seismic ambient noise obtained from the Field Test in Felsőpetény (Hungary) in 2019, the karst and clay-mining area. The noise was recorded at 50 points distributed in the area over a known cavity with the ceiling at 70 m depth. Using our method, we were able to locate the horizontal position of the cavity in the aerial maps of the Finite-interval Spectral Power of the recorded seismic ambient noise.

The method is ready for further tests in different cavity conditions and applications.

## DATA AND RESOURCES

Data used in this study was obtained by a group of staff and invited experts during the Field Test of OSI Geophysical Techniques for Deep Applications in Hungary, 11-20 September 2019. Measurements were conducted using fifty 3-component Lennartz seismometers and fifty Reftek 130 digitizers. The data was made available upon request from the Provisional Technical Secretariat and with the consent of the Hungarian authorities.

1  
2     ACKNOWLEDGMENTS  
3  
4  
5  
6  
7  
8  
9  
10  
11  
12  
13  
14  
15  
16  
17  
18  
19  
20

We thank the Provisional Technical Secretariat for organizing the field test in Hungary and for the provision of resulting data. We also thank to the Hungarian host representatives, particularly Endre Hegedus and Attila Kovacs, for their support. We thank Gregor Malich, Chief of the Equipment and Implementation Section, OSI Division, CTBTO, for the critical reading of the manuscript. We greatly appreciate constructive comments and suggestions by anonymous reviewers. They helped to improve the paper. We also thank Dr. Samuel Toon from CTBTO for useful discussion during revision of the original manuscript. This work was supported by the Slovak Research and Development Agency under the contract APVV-15-0560 (project ID-EFFECTS). This work was also partially supported by the Slovak Foundation Grant VEGA-2/0046/20.

21  
22  
23  
24  
25     REFERENCES  
26  
27  
28  
29

Albarello, D., & Lunedei, E. 2013. Combining horizontal ambient vibration components for H/V spectral ratio estimates. *Geophys. J. Int.*, **194**, 936–951.

Bard, P.-Y., Acerra, C., Alguacil, G., Anastasiadis, A., Atakan, K., Azzara, R., Basili, R., Bertrand, E., Bettig, B., Blarel, F., Bonnefoy-Claudet, S., Bordoni, P., Borges, A., Böttger-Sørensen, M., Bourjot, L., Cara, F., Caserta, A., Chatelain, J.-L., Cornou, C., Cotton, F., Cultrera, G., Daminelli, R., Dimitriu, P., Dunand, F., Duval, A.-M., Fäh, D., Fojtikova, L., de Franco, R., di Giulio, G., Grandison, M., Guéguen, P., Guillier, B., Haghshenas, E., Havskov, J., Jongmans, D., Kind, F., Kirsch, J., Koehler, A., Koller, M., Kristek, J., Kristekova, M., Lacave, C., La Rocca, M., Marcellini, A., Maresca, R., Margaris, B., Moczo, P., Moreno, B., Morrone, A., Ohrnberger, M., Ojeda, J.A., Oprsal, I., Pagani, M., Panou, A., Paz, C., Querendez, E., Rao, S., Rey, J., Richter, G., Rippberger, J., Roquette, P., Roten, D., Rovelli, A., Saccorotti, G., Savvaidis, A., Scherbaum, F., Schisselé, E., Spühler-Lanz, E., Tento, A., Teves-Costa, P., Theodulidis, N., Tvedt, E., Utheim, T., Vassiliadès, J.-F., Vidal, S., Viegas, G., Vollmer, D., Wathélet, M., Woessner, J., Wolff, K., & Zacharopoulos, S. 2004. Guidelines for the implementation of the H/V spectral ratio technique on ambient vibrations measurements, processing and interpretation. Deliverable D23.12 of the SESAME project, 62 pp, December 2004. Available at [http://sesame.geopsy.org/Papers/HV\\_User\\_Guidelines.pdf](http://sesame.geopsy.org/Papers/HV_User_Guidelines.pdf)

Bonnefoy-Claudet, S., Cornou, C., Bard, P.-Y., Cotton, F., Moczo, P., Kristek, J., & Fäh, D. 2006. H/V ratio: a tool for site effects evaluation. Results from 1-D noise simulations. *Geophys. J. Int.*, **167**(2), 827-837.

- 1  
2 Filippi, C., Leparoux, D., Grandjean, G., Bitri, A., & Cote, P. 2019. New robust observables  
3 on Rayleigh waves affected by an underground cavity: from numerical to experimental  
4 modelling. *Geophys. J. Int.*, **218**(3), 1903-1918.  
5  
6 Guidoboni, E., Mariotti, D., Giammarinaro, M. S., & Rovelli, A. 2003. Identification of  
7 amplified damage zones in Palermo, Sicily (Italy), during the earthquakes of the last three  
8 centuries. *Bull. Seism. Soc. Am.*, **93**(4), 1649-1669.  
9  
10 Kolesnikov, Y. I., & Fedin, K. V. 2018. Detecting underground cavities using microtremor  
11 data: physical modelling and field experiment. *Geophysical Prospecting*, **66**(2), 342-353.  
12  
13 Konno, K., & Ohmachi, T. 1998. Ground-motion characteristics estimated from spectral ratio  
14 between horizontal and vertical components of microtremor. *Bull. Seism. Soc. Am.*,  
15 **88**(1), 228-241.  
16  
17 Korneev, V. 2009. Resonant seismic emission of subsurface objects. *Geophysics*, **74**(2), T47-  
18 T53.  
19  
20 Korneev, V., Gritto, R., Magomedov, M., Zuev, M., Elobaid, E. A., & Sadooni, F. N. 2014.  
21 Seismic detection of a sinkhole using spectral-based analysis. In *SEG Technical Program  
22 Expanded Abstracts 2014* (pp. 2140-2144): Society of Exploration Geophysicists.  
23  
24 Kristek, J., Kristekova, M., Moczo, M., & Galis, M. 2019. Report on identification of  
25 significant changes in seismic wavefields. *Report to CTBTO*, January 2019. 105pp.  
26  
27 Kristekova, M., Kristek, J., Moczo, P., Labak, P., & Galis, M. 2019. Numerical modeling of  
28 seismic wavefields in media modified by an underground nuclear explosions and  
29 identification of cavity. *Seismol. Res. Lett.*, **90**(2B), 992.  
30  
31 Moczo, P., & Kristek, J. 2002. FD code to generate noise synthetics, *Deliverable of the  
32 SESAME European Project*, D09.02.  
33  
34 Ortiz-Aguilar, S., De Basabe, J. D., Gonzalez-Escobar, M., & Magar, V. 2020. Theoretical  
35 signature of a cavern created by an Underground Nuclear Explosion in 2D exploration  
36 seismic data. *Geophys. J. Int.*, **221**(3), 1789-1801.  
37  
38 Schneider, F. M., Esterhazy, S., Perugia, I., & Bokelmann, G. 2017. Seismic resonances of  
39 spherical acoustic cavities. *Geophys. Prosp.*, **65**, 1-24.  
40  
41 Sgarlato, G., Lombardo, G., & Rigano, R. 2011. Evaluation of seismic site response nearby  
42 underground cavities using earthquake and ambient noise recordings: A case study in  
43 Catania area, Italy. *Engineering Geology*, **122**(3), 281-291.  
44  
45 Sica, S., Dello Russo, A., Rotili, F., & Simonelli, A. L. 2014. Ground motion amplification due  
46 to shallow cavities in nonlinear soils. *Natural Hazards*, **71**(3), 1913-1935.  
47  
48 Sweeney, J. J., & Harben, P. 2010. *OSI Passive Seismic Experiment at the Former Nevada Test  
49 Site*. Retrieved from United States: <https://www.osti.gov/servlets/purl/1018759>

1  
2 Sweeney, J. J., & Mellors, R. J. 2014. *Application of Active Seismic and Electrical Methods to*  
3 *Detect and Characterize Subsurface Effects of an Underground Explosion.* Retrieved  
4 from United States: <https://www.osti.gov/servlets/purl/1129148>

5  
6  
7 Tukey, J. W. 1977. *Exploratory data analysis.* Reading, Mass.; London: Addison-Wesley.  
8  
9  
10  
11  
12  
13  
14  
15  
16  
17  
18  
19  
20  
21  
22  
23  
24  
25  
26  
27  
28  
29  
30  
31  
32  
33  
34  
35  
36  
37  
38  
39  
40  
41  
42  
43  
44  
45  
46  
47  
48  
49  
50  
51  
52  
53  
54  
55  
56  
57  
58  
59  
60